Journal of Heat and Mass Transfer Research

Journal homepage: https://jhmtr.semnan.ac.ir

Semnan University

ISSN: 2383-3068

Research Article

Synthesis of TiO_2 Nanoparticles and Investigation of Heat Transfer and Exergetic Performance of a Shell and Tube Heat Exchanger with TiO_2-PGW Nanofluid

Gogan Dhar , M. A. Mowazzem Hossain * , Uschuas Dipta Das

Department of Mechanical Engineering, Chittagong University of Engineering and Technology, Chattogram- 4349, Bangladesh

ARTICLE INFO

Article history:

Received: 2025-04-20

Revised: 2025-06-15

Accepted: 2025-06-30

Keywords:

TiO_2 nanoparticles;

Nanofluid;

Propylene glycol-water;

Exergy;

Heat transfer.

ABSTRACT

In this experimental study, titanium dioxide (TiO_2) nanoparticles were synthesized using an ultrasound-assisted technique. The structural as well as morphological characteristics of the produced TiO_2 nanoparticles were studied through X-ray diffraction (XRD) and scanning electron microscopy (SEM). Heat transfer, as well as exergetic parameters of propylene glycol-water (PGW)-based TiO_2 nanofluid in a shell-and-tube heat exchanger, were then explored. The nanofluid was made ready by mixing 60% water and 40% propylene glycol, incorporating TiO_2 nanoparticle concentrations of 0.1 vol.%, 0.2 vol.%, and 0.3 vol.% through a two-step process. The flow rate of the nanofluid was varied between 6–12 l/min, while the flow rate of the hot water was maintained at 12 l/min. The study revealed that increasing both the flow rate and nanoparticle concentration of the nanofluid significantly improved the heat transfer rate ($\dot{Q}$) as well as the overall heat transfer coefficient (U). Specifically, at a nanoparticle concentration of 0.3 vol.% and a flow rate of 12 l/min, the heat transfer rate increased by 44.3%, and the heat transfer coefficient increased by 46.1%. Furthermore, the average effectiveness of the heat exchanger improved with nanoparticle concentrations of 0.1 vol.%, 0.2 vol.%, and 0.3 vol.%, showing increases of 11.91%, 29.88%, and 41.82%, respectively. The research also indicated that exergy loss as well as the dimensionless exergy loss initially increased with higher nanoparticle concentrations but then decreased as the concentration continued to rise. Notably, at a concentration of 0.3 vol.% and a nanofluid flow rate of 6 l/min, the highest exergetic sustainability index (0.44) and the lowest environmental impact factor (2.3) were observed.

1. Introduction

The rapid increase in climate change, global warming, the effect of greenhouse gases, and the growing energy demand have led the modern world to make every effort to save and effectively transfer energy. A heat exchanger, which makes energy transfer across various media easier, is a crucial tool in this endeavor. In energy conversion systems, heat exchangers are essential components. The thermal and physical characteristics of heat transfer fluids are important variables that affect the heat exchanger's performance [1–4]. The most commonly used form of heat exchanger among the several types is the shell and tube heat exchanger, which finds usage in a variety of industrial applications such as energy

* **Corresponding author.**

E-mail address: *mowazzem@cuet.ac.bd*

Cite this article as:

Dhar G., Hossain, M.A. M. and Das, U. D., 2026. Synthesis of TiO_2 Nanoparticles and Investigation of Heat Transfer and Exergetic Performance of a Shell and Tube Heat Exchanger with TiO_2-PGW Nanofluid. . *Journal of Heat and Mass Transfer Research*, 13(2), pp. 229-244.
https://doi.org/10.22075/JHMTR.2025.37422.1725

conversion, evaporation, condensation, heating, cooling, ventilating, power utility systems, and air conditioning engineering [5]. Researchers have been attempting to increase the heat transfer rates of heat exchangers, reduce their size, weight, and cost, minimize energy losses, and improve energy and fuel efficiency. There are several approaches to augment the effectiveness of heat exchangers, including the incorporation of fins, the use of microchannels, and the expansion of the heat transfer area. Furthermore, increasing the thermal conductivity of the working fluid plays a significant role in enhancing heat transfer efficiency [6]. Common fluids, such as water, refrigerants, motor oil, paraffin oil, propylene glycol, ethylene glycol, and vegetable oil, typically exhibit lower thermal conductivities compared to solid materials. One method that researchers have explored to enhance thermal conductivity is the addition of solid particles with higher thermal conductivity to a base fluid [7]. However, suspended particles, whether micrometer or millimeter-sized, can lead to several significant issues, such as clogging, abrasion, high-pressure drops, and particle sedimentation. Despite thia, nanoparticles, having an average size of less than 100 nm, are used to avoid these issues [8,9]. Among their various technical applications, nanofluids—suspensions of colloidal nanoparticles in a base fluid—are anticipated to replace conventional fluids soon [10, 11]. Notably, metal oxide nanoparticles are generally inexpensive and easy to synthesize. In this experimental study, TiO2 nanoparticles have been synthesized using a modified sulfuric acid method through ultrasound [12].

Nanofluids are created by dispersing selected nanoparticles in a base fluid at varying concentrations. Ethylene glycol (EG) or propylene glycol (PG) are commonly used as an antifreeze, with PG being preferred in food applications due to its safety despite having lower physical properties than EG [13]. Although thermal conductivity is a primary contributor to improving heat transfer in nanofluids, it is not the only mechanism. Due to the motion of the nanoparticles, which can result in micro-convection effects and improved momentum exchange within the fluid, nanofluids also show improved convective heat transfer. If precise thermophysical characteristics are applied, single-phase Nusselt number correlations can frequently be used to characterize this behavior. The experimental research conducted by Buschmann et al. [14] shows that Newtonian nanofluids exhibit consistent heat transfer patterns devoid of unusual behaviors, and the improvement seen is correlated with better particle dynamics and thermal conductivity. Furthermore, according to Aksoy et al. [15], nanofluid sprays improve heat transfer by primarily coating the heated surface and then continually self-sustaining the optimal coating due to the continuous deposition of nanoparticles. Hamilton [16] presented a model of thermal conductivity for a two-phase mixture based on theoretical research. The term "nanofluid" to describe fluids containing suspended nanoparticles was introduced by Choi [17]. In comparison with water without nanoparticles, a concentration of 5 vol.% water-based CuO nanofluid can raise its thermal conductivity by 60%, as suggested by Li et al. [18]. Masuda et al. [19] suggested that the thermal conductivities of liquid-dispersed ultra-fine particles, specifically Al_2O_3 and TiO_2 at a concentration of 4.3 vol.%, were enhanced by approximately 32% and 11%, respectively. For EG and PG-based TiO_2 nanofluids, Cabaleiro et al. [20] investigated thermal conductivity at nanoparticle concentrations of up to 8.5 vol.%, reporting an increase in thermal conductivity of up to 15.4%. In addition, anatase nanocrystalline nanofluids demonstrated slightly better enhancements. Sundar et al. [21] observed the thermal as well as rheological properties of PGW-based Fe_3O_4 nanofluids, noting a thermal conductivity increment of 20.53% and 17.26% for 20:80% and 40:60% PG/water nanofluids, respectively, at a particle concentration of 0.5 vol.% along with a temperature of 60°C. Hussein et al. [22] investigated the use of water-based TiO_2 and SiO_2 nanofluids to enhance heat transfer in automobile radiators. Their results indicated that heat transfer improves as the volume concentration of the nanofluid increases. Devireddy et al. [11] analyzed EGW-based TiO_2 nanofluids as automotive radiator coolants, using a 60% water and 40% ethylene glycol mixture with TiO_2 concentrations of 0.1 vol.%, 0.3 vol.%, and 0.5 vol.%. They found a maximum rate of heat transfer increase of 37% compared to the base fluid. In a different research, Palanisamy and Kumar [23] found that with a cone helically coiled tube heat exchanger, the Nusselt numbers for water-based multi-walled carbon nanotube (MWCNT) nanofluids at 0.1 vol.%, 0.3 vol.%, and 0.5 vol.% concentrations were, respectively, 28%, 52%, and 68% higher compared to water. According to Jagadishwar and Babu [24], PGW-based TiO_2 nanofluids were tested in an automotive radiator at different flow rates with concentrations of 0.1 vol.%, 0.2 vol.%, and 0.35 vol.%. At specific concentrations and flow rates, they showed that the heat transfer rate rose as the flow rate increased.

In order to improve the performance of the disc-and-doughnut shell-and-tube heat exchangers (STHXs), Mohammadzadeh et al. [25] investigated several tube geometrical

arrangement configurations along with the inclusion of ternary nanoparticles. In comparison to the triangular 30° STHX, the study demonstrated that the heat transfer to pressure drop ratio increased by 79.73% at a mass flow rate of 1.6 kg/s. The fluid with a ternary nanoparticle concentration of 5% performed the best among all those tested. Heat transfer improved with an increase in the volume fraction of nanoparticles, but pressure drop also increased. Shell-and-Tube Heat Exchangers (STHE) are essential in many industrial applications, as examined by Mohammadzadeh et al. [26] in another study. For baffles angled between 0° and 30°, the results showed that the pressure drop in the shell section increased by 56.8 to 60.9%. There was also a higher total heat transfer coefficient, by about 4.5–6% for the 30° inclined baffles compared to the 0° inclined baffles. A 3D numerical study of the melting behavior of a phase changing material (PCM) in a helix-shaped coil-tube heat exchanger was conducted by Khedher et al. [27]. According to the results, central return tube layouts improved charging capacity and beginning melting rates when compared to a typical coil. After 5000 s from the start of melting, the top inlet design outperformed the bottom inlet by 16.5% in melting rate. In contrast to the traditional system, the arrangement with the central return tube at the top showed incremental gains in energy storage of 18.8%, 13.1%, and 1.9% for operational time intervals of 1000, 5000, and 10,000, respectively. Paikar et al. [28] demonstrated that the pressure drop and heat transfer coefficient within the shell-and-tube heat exchanger (STHE) tubes were enhanced by the use of single and double-blade turbulators (SBT and DBT). For instance, the heat transfer coefficient improved by 25.41% and 33.43%, respectively, when SBT and DBT were employed at a mass flow rate of 0.338 kg/s. Furthermore, compared to the base model (heat exchanger without a turbulator), the pressure drops with the SBT and DBT increased by 6.32 and 8.62 times, respectively, at a mass flow rate of 0.45 kg/s. To evaluate the performance of phase change materials (PCMs), Moghaddam et al. [29] conducted a study that focused on two aspects: the incorporation of fins and the use of porous media during the melting process within a triple-concentric-tube heat exchanger. The importance of shell-and-tube heat exchangers (STHX) was examined by Mohammadzadeh et al. [30], focusing on various types of baffles, including segmental, double segmental, helical, disc-and-doughnut, clamping anti-vibration, and Flower-B. Their study demonstrated that using clamping anti-vibration, Flower-B, helical, and double segmental baffles reduced the shell side pressure drop by 14% to 28%. Although these designs resulted in lower overall heat transfer coefficients, the disc-and-doughnut baffles achieved higher overall heat transfer coefficients—ranging from 21% to 24%—compared to segmental baffles.

Exergy is the maximum useful work a reversible system can deliver in a given environment [31,32]. The second law of thermodynamics analysis, or exergy analysis, is key to understanding the thermodynamic behavior of heat exchangers. This method combines the second law of thermodynamics with mass and energy conservation to evaluate energy systems [33].

In a developing country like Bangladesh, the energy crisis is a significant concern. To effectively address this issue, accurate information on energy consumption and losses is crucial. Traditional energy analysis focuses on the quantity of energy used and lost, while neglecting the quality and internal inefficiencies of the equipment, which makes it increasingly inadequate [34,3]. Conversely, exergy analysis provides insights into the usable work potential of a system. By assessing exergy losses, it allows for a better evaluation of process inefficiencies and can indicates whether design improvements could reduce inefficiencies in energy systems [35].

Due to its significant potential in sustainable energy, exergy analysis has become a major area of study worldwide [36]. Durmuş [37] investigated heat transfer, pressure loss, and exergy both with and without cut-out conical turbulators in a heat exchanger, deriving and discussing several empirical correlations to describe the results. The effects of flow, thermodynamic as well as geometrical factors, on the exergetic performance of a tube-in-tube helically coiled (TTHC) heat exchanger were studied by Dizaji et al. [38]. Their experimental investigation showed that increasing flow rates, coil diameter, and the temperature of the hot fluid input led to an increase in energy loss. Utilizing CuO/water nanofluids, Khairul et al. [39] looked into the exergy loss in a corrugated plate heat exchanger. They discovered that exergy destruction was reduced by 24%, 16.25%, and 8% compared to water for nanoparticle concentrations of 1.5 vol.%, 1.0 vol.%, and 0.5 vol.%, respectively. Esfahani and Languri [40] examined the exergetic effectiveness of a shell-and-tube heat exchanger with graphene oxide nanofluid at concentrations of 0.01 wt.% and 0.1 wt.%. They found that distilled water brought about 22% and 109% more exergy loss compared to nanofluids having concentrations of 0.01 wt.% and 0.1 wt.%, respectively, under laminar flow conditions.

Despite numerous prior studies evaluating the performance of heat exchangers, there remains a limited understanding of how the PGW mixer affects heat transfer as well as exergetic performance in shell-and-tube heat exchangers. This research began with the fabrication and characterization of TiO_2 nanoparticles. The subsequent analysis focused on the heat transfer as well as the exergetic efficiency of the shell-and-tube heat exchanger by varying the flow rates and nanoparticle volume concentrations of a PG and water-based TiO_2 nanofluid.

2. Experimentation

2.1. Materials

TiO_2 powders were purchased from Taj Scientific, Chittagong, Bangladesh (manufactured by PT. Smart-Lab, Indonesia). The Postgraduate Laboratory of the Department of Physics, CUET, provided 98% H_2SO_4 and 25% NH_4OH solution.

2.2. TiO_2 Nanoparticle Preparation and Characterization

In this study, TiO_2 nanoparticles were prepared using an ultrasound-assisted method [12]. The procedure was modified to align with available lab facilities and to enhance cost-effectiveness. To prepare the precursor for the TiO2 nanoparticles, 20 grams of anatase TiO_2 particles were placed in a 500 ml beaker. Then, 40 ml of 98% sulfuric acid (H_2SO_4) was added dropwise to the TiO_2 particles in the beaker. The mixture was then subjected to ultrasound treatment at a frequency of 40 kHz for 45 minutes in an ultrasonic bath. This was followed by heating the beaker at 100 °C in an oven. The ultrasonic waves created intense mixing and facilitated the reaction between TiO_2 and H_2SO_4 [12]. This process helped to break down the chemical bonds in the TiO_2 particles and form new structures at elevated temperatures (Eq. 1). After adding distilled water to the beaker, the mixture was stirred for five minutes using a glass rod. Ammonium hydroxide solution (25%) was then used to adjust the pH to a range of 8 to 11. The solution was filtered through filter paper to remove by-products. After filtering, the product was washed and filtered three additional times. Subsequently, the sample was transferred to another beaker and dried at 30 °C for 30 minutes in a water bath. The final product was then calcined, or annealed, for two hours at a temperature of 500 °C. The complete TiO_2 nanoparticle synthesis procedure is depicted in Figure 1. After calcination, the final product was thoroughly crushed utilizing a mortar and pestle. Figure 2 illustrates several important steps in the synthesis of the nanoparticles.

The possible chemical reactions during the interaction of TiO_2 with H_2SO_4 are shown in the following equations (1–4) [12]:

$$TiO_2 + 2H_2SO_4 \xrightarrow[+\ 100\ ^\circ C]{\text{Ultrasonic energy}} H_2[TiO(SO_4)_2] + H_2O \quad (1)$$

$$H_2[TiO(SO_4)_2] \rightarrow TiOSO_4 + H_2SO_4 \quad (2)$$

$$TiOSO_4 + (n+1)H_2O \rightarrow TiO_2.nH_2O + H_2SO_4 \quad (3)$$

$$TiO_2.nH_2O \rightarrow TiO_2 + nH_2O \quad (4)$$

The crystal structure as well as the microstructure of the fabricated TiO_2 nanoparticles were studied using XRD (GBC Scientific; Cu_Kα1: λ = 1.54062 Ao radiation source) and SEM (Hitachi S3400N) analysis.

In this study, the crystallite size of the particles has been estimated by using the Debye-Scherer formula as presented in Eq. (5):

$$D = \frac{k\,\lambda}{\beta\cos\theta} \quad (5)$$

where D is the crystallite size, k is the Scherrer constant (0.89), λ is the X-ray wavelength (0.15406 nm), β is FWHM (full width at half maximum), and θ is the diffraction angle.

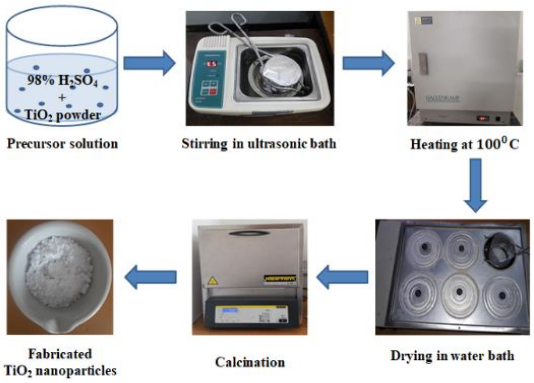

Fig. 1. Schematic representation of TiO_2 nanoparticles synthesis process

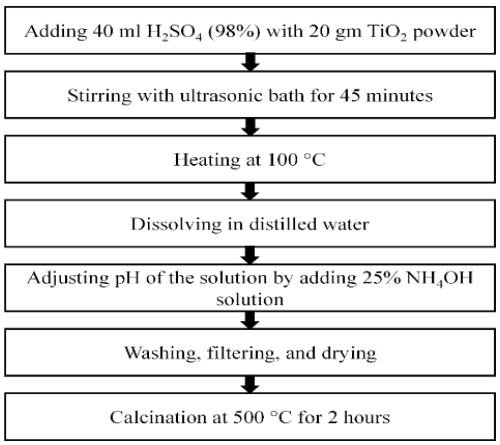

Fig. 2. A flow diagram showing how TiO_2 nanoparticles are made utilizing the modified H_2SO_4 technique with ultrasonic assistance

The d-space, or interplanar separation between atoms, was computed using Bragg's Law as shown in Eq. (6).

$$2d \sin\theta = n\lambda \quad (6)$$

where, d is inter-planar spacing.

The crystal system of anatase TiO_2 nanoparticles is tetragonal-body centered. The following formulas in Eq. (7) and Eq. (8) were utilized to calculate the lattice parameters (a = b and c) and the volume (V) of the nanoparticles' unit cell using Miller indices (hkl) and d-spacing:

$$\frac{1}{d^2} = \frac{h^2 + k^2}{a^2} + \frac{l^2}{c^2} \quad (7)$$

$$V = a^2 c \quad (8)$$

2.3. Preparation of TiO_2 Nanofluid

TiO_2 nanofluid was prepared in this work utilizing a two-step process that involved adding varying volume percentages of TiO_2 nanoparticles to a base fluid consisting of 40% PG and 60% water. To make nanofluids, the amount of nanoparticles required was calculated using the law of mixing. With a propylene glycol-water mixture (PGW) (40:60) as a base fluid, the weight of the nanoparticles needed for producing the nanofluid of a specific volume fraction was determined using the following Eq. (9) [3]:

$$\%\ \text{vol. concentration},\quad \varphi = \frac{\frac{w_{nanoparticle}}{\rho_{nanoparticle}}}{\frac{w_{nanoparticle}}{\rho_{nanoparticle}} + \frac{w_{base\ fluid}}{\rho_{base\ fluid}}} \quad (9)$$

The required amount of TiO_2 nanoparticles for a specified concentration was dissolved in a 1 L PGW mixture. The solution was then mixed for 10 hours using a magnetic stirrer, followed by 1 hour of sonication in an ultrasonic bath. A total of 5 l of nanofluid with specific volume concentrations was prepared. The investigation utilized TiO2 nanoparticles at concentrations of 0.1 vol.%, 0.2 vol.%, and 0.3 vol.%. The necessary components and the procedure for nanofluid preparation are depicted in Figure 3.

Equations (10–13) derived by Pak and Cho [41] were utilized to calculate the density, specific heat, and thermal conductivity of the materials involved. The thermal characteristics of the base fluid, water, and the nanoparticles are presented in Table 1 [21, 42–46].

$$\rho_{nf} = \varphi\rho_{np} + (1-\varphi)\rho_{bf} \quad (10)$$

$$C_{p,nf} = \frac{\varphi(\rho Cp)_{np} + (1-\varphi)(\rho Cp)_{bf}}{\rho_{nf}} \quad (11)$$

$$\mu_{nf} = \mu_{bf}(1 + 2.5\varphi + 6.2\varphi^2) \quad (12)$$

$$K_{nf} = K_{bf}\frac{K_{np} + 2K_{bf} - 2\varphi(K_{bf} - K_{np})}{K_{np} + 2K_{bf} + \varphi(K_{bf} - K_{np})} \quad (13)$$

Table 1. Thermal characteristics of TiO_2 nanoparticle, water, and base fluid

Material	Density (kg/m³)	Specific heat (J/Kg K)	Thermal conductivity (W/m K)
TiO_2	3895	689.62	8.5
Water	998.9	4181	0.613
PGW (40:60)	1026.5	3747.186	0.388

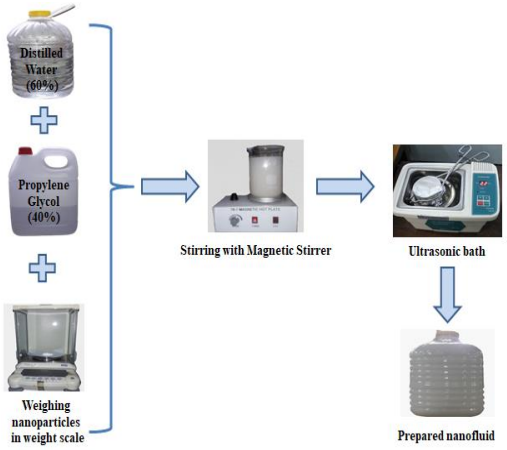

Fig. 3. Nanofluid preparation procedure

2.4. *Experimental Setup and Procedure*

This study utilized a shell-and-tube heat exchanger of the NFU type, as defined by TEMA (Tubular Exchanger Manufacturers Association) nomenclature © 1988. The "N" indicates a channel with a removeable cover and tube sheet, "F" denotes a longitudinally baffled two-pass shell, and "U" refers to the U-tube bundle. The heat exchanger consisted of two stainless steel tubes, each with an inner diameter of 0.009 meters, an outer diameter of 0.0095 meters, and a length of 0.49 meters. The cylindrical shell had a length of 0.3045 meters and an outer diameter of 0.15 meters. It utilized a parallel-flow arrangement, as shown in the SolidWorks model in Figure 4.

The experimental setup was designed to assess the exergetic performance and heat transfer rate of a shell-and tube heat exchanger. The setup included two 0.5-hp centrifugal pumps (RFL Water Pump, Centrifugal 1"X1"-0.5 HP (RCm-130)), two flow measurement devices (PRM FMZ400410 GPM 1-10 GPM Water Rotameter Flow Meter with ± 4% accuracy), two flow regulator valves, and various pipes, joints, and other components. Additionally, the setup featured a cold fluid storage tank and an electric heater for hot fluid storage. To minimize heat loss between the test apparatus and the surrounding

air, glass wool, insulating tape, and aluminum foil were used for insulation. The details of the water pumps that were utilized in the experiment are shown in Table 2. A schematic diagram and a photograph of the experimental setup are shown in Figures 5 and 6, respectively.

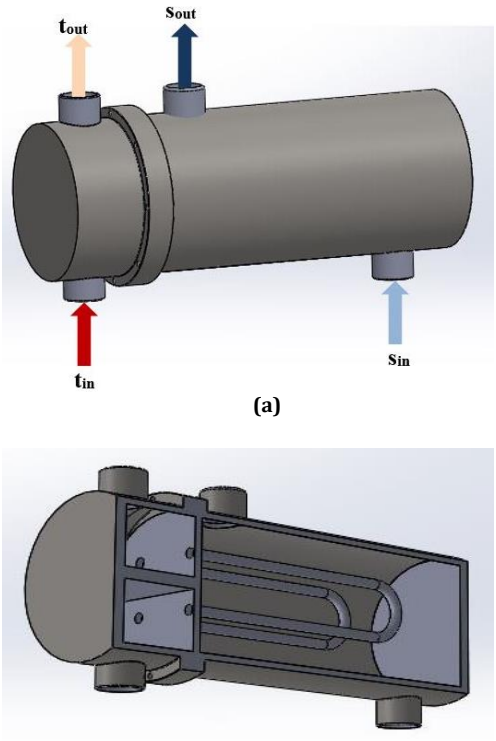

Fig. 4. Solidworks model of the test section (a) Shell-and-tube heat exchanger model with flow directions; (b) Section view of a heat exchanger

Table 2. Details of the water pumps that were used in this experimental study

Specifications	Value
Model	BBY03343
Motor power	0.5 hp (0.37 KW)
Motor voltage	220 V
Max. head	24 m
Max. flow rate	50 l/min
Sn.	1 inch
Dn.	1 inch

A closed-loop heat exchanger was connected to two buckets, as depicted in Figure 6. One bucket contained hot water, heated by an electric heater, while the other contained a nanofluid serving as the coolant. Two separate pumps were employed to circulate the nanofluid and hot water through a 1-inch-diameter conduit. The shell side was designated for the circulation of the nanofluid, whereas the tube side was utilized for the hot water. To measure the Volumetric flow rate, two flow meters (rotameters) were installed in the loop. Flow rates were adjusted using gate valves, maintaining a steady flow of 12 liters per minute for the hot fluid. The nanofluid flow rates were varied at 6, 8, 10, and 12 liters per minute. Four nitrogen-filled laboratory thermometers (ZEAL, manufactured in England; range: -10 to 110 °C with a precision of ± 0.1 °C) were positioned on the pipe at both the entrance and exit of the hot water and nanofluid to monitor the necessary temperatures. Data collection occurred during a sustained flow period.

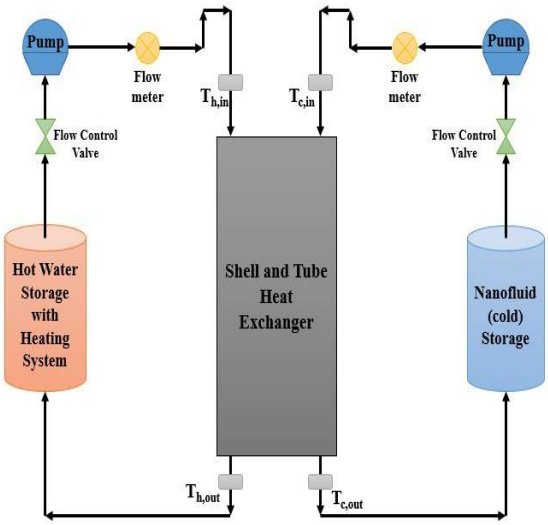

Fig. 5. Schematic diagram of the experimental setup

2.5. Calculation Method

2.5.1. Thermal Performance

The heat transfer rate of the nanofluid (cold fluid) can be estimated using the following Eq. (14) [47]:

$$\dot{Q}_c = \dot{m}_c C_{pc}(T_{c,out} - T_{c,in}) \quad (14)$$

where, $\dot{m}_c$ is the mass flow rate, C_{pc} is the specific heat, $T_{c,in}$ and $T_{c,out}$ are the inlet and outlet temperatures of the nanofluid, respectively.

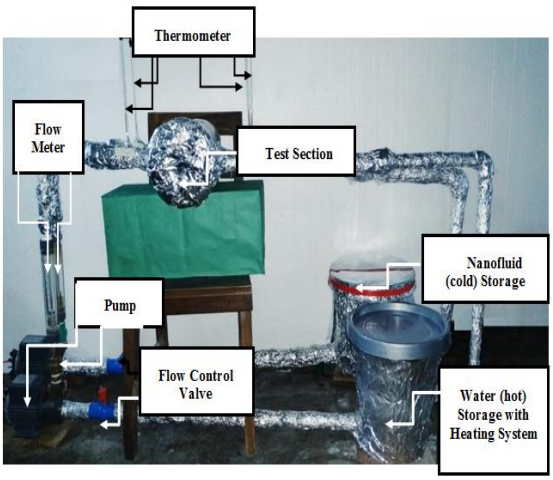

Fig. 6. Image of the experimental setup

Now, the U of nanofluid can be calculated by Eq. (15):

$$U_0 = \frac{\dot{Q}_c}{A_o\, F\, \Delta T_m} \tag{15}$$

where, ΔT_m is the log mean temperature difference (LMTD), A_0 is the total tube area (outer side), and F is the LMTD correction factor that can be obtained from a chart using two parameters P and R [47].

The effectiveness of an NFU type shell-and-tube heat exchanger can be estimated using the following Eq. (16) [47]:

$$\varepsilon = \frac{\text{Actual heat transfer rate}}{\text{Maximum possible heat transfer rate}} = \frac{\dot{Q}}{Q\dot{m}ax} \tag{16}$$

where,

$$\dot{Q} = \dot{m}cC_{pc}\dot{(T_{c,out} - T_{c,in})} = \dot{m}hC_{ph}(T_{h,out} - T_{h,in}) \tag{17}$$

$$Q_{max} = C_{min}(T_{h,in} - T_{c,in}) \tag{18}$$

here, C_{min} = The smaller of $\dot{m}_cC_{pc}$ and $\dot{m}_hC_{ph}$

2.5.2. Exergy Analysis

The exergy balance for a certain steady-state control volume may be expressed as follows:

$$\sum E_{in} = \sum E_{out} - \sum E_{product} \tag{19}$$

The following formula (Eq. (20)) can be used to determine the exergy loss of a steady-state open system:

$$E = E_h + E_c \tag{20}$$

where, the following Eq. (21) [38] can be used to represent Eh and Ec, which stand for the energy change of the hot and cold fluids, respectively:

$$E = T_e\left[\dot{m}_hC_{ph}\ln\left(\frac{T_{h,out}}{T_{h,in}}\right) + \dot{m}_cC_{pc}\ln\left(\frac{T_{c,out}}{T_{c,in}}\right)\right] \tag{21}$$

The assessment of dimensionless exergy loss was conducted by normalizing the exergy loss in relation to the availability of the hot fluid stream using Eq. (22) [38]. In alignment with established research methodologies, a reference environment of 298 K and 1 atm was employed. This approach ensures both standardization and comparability across the evaluation.

$$e = \frac{\mathrm{E}}{\dot{\mathrm{m}}_{\mathrm{h}}\, C_{ph}\left\{\Delta T_h - T_e\left[\ln\left(\frac{T_{h,out}}{T_{h,in}}\right)\right]\right\}} = \frac{\mathrm{E}}{\dot{\mathrm{m}}_{\mathrm{h}}\, C_{ph}\left\{(T_{h,in} - T_{h,out}) - T_e\left[\ln\left(\frac{T_{h,out}}{T_{h,in}}\right)\right]\right\}} \tag{22}$$

When energy is exchanged in a heat exchanger from a fluid stream with a higher temperature to one with a lower temperature, the second law efficiency, also known as the exergetic effectiveness, is described as following the Eq. (23) [38]:

$$\eta = \frac{\dot{\mathrm{m}}_{\mathrm{c}}\,(\Psi_{\mathrm{c,out}} - \Psi_{\mathrm{c,in}})}{\dot{\mathrm{m}}_{\mathrm{h}}\,(\Psi_{\mathrm{h,in}} - \Psi_{\mathrm{h,out}})} = \frac{\dot{\mathrm{m}}_{\mathrm{c}}\, \mathrm{C}_{\mathrm{pc}}\left\{(\mathrm{T}_{\mathrm{c,out}} - \mathrm{T}_{\mathrm{c,in}}) - \mathrm{T}_{\mathrm{e}}\left[\ln\left(\frac{\mathrm{T}_{\mathrm{c,out}}}{\mathrm{T}_{\mathrm{c,in}}}\right)\right]\right\}}{\dot{\mathrm{m}}_{\mathrm{h}}\, \mathrm{C}_{\mathrm{ph}}\left\{(\mathrm{T}_{\mathrm{h,in}} - \mathrm{T}_{\mathrm{h,out}}) - \mathrm{T}_{\mathrm{e}}\left[\ln\left(\frac{\mathrm{T}_{\mathrm{h,in}}}{\mathrm{T}_{\mathrm{h,out}}}\right)\right]\right\}} \tag{23}$$

The reference temperature and pressure were taken as 298 K (the standard ambient conditions) and atmospheric pressure, respectively.

2.5.3. Sustainability and Environmental Impact Analysis

In order to achieve sustainable development, it is essential to use sustainable energy resources effectively. The environmental impact of energy processes is closely tied to exergy analysis. In thermodynamically ideal and reversible processes, there are no exergy losses, resulting in an exergy efficiency of 1 (or 100%) and no negative environmental effects; these processes are fully sustainable. Conversely, in actual irreversible processes, exergy is destroyed, leading to losses. As exergy efficiency approaches zero, sustainability diminishes, and environmental impact increases significantly. By enhancing exergy efficiency, we can promote longer-term development while reducing environmental effects. When exergy efficiency approaches 100%, sustainability becomes nearly limitless, and environmental impacts are minimized. The process nears reversibility when exergy is converted from one form to another without any losses [49].

The exergetic sustainability index (SI) is a valuable metric for evaluating the sustainability of energy processes and is commonly employed to quantify exergy performance in various applications [48]. The sustainability index can be estimated using established methodologies, as outlined in Eq. (24) [49].

$$SI = \frac{\eta}{1 - \eta} \tag{24}$$

Conversely, the environmental impact factor (EIF) helps to determine the extent to which a system's exergy losses may affect the environment. A system with a lower EIF is more ecologically friendly. The following Eq. (25) [49] can be used to calculate the environmental impact factor:

$$EIF = \frac{1}{SI} \tag{25}$$

3. Results and Discussion

3.1. XRD Analysis

The XRD pattern of the synthesized TiO_2 nanoparticles is presented in Figure 7, with detailed peak information summarized in Table 3. The XRD analysis confirms that the produced TiO_2 nanoparticles exhibit a tetragonal anatase structure. This pattern is consistent with JCPDS data (PDF No: 21-1272) as well as findings from other experimental studies [50, 51]. Notable peaks appear at 2θ values of 25.4°, 37.06°, 37.91°, 38.67°, 48.15°, 53.96°, 55.16°, 62.78°, 68.84°, and 70.356°, corresponding to the (101), (103), (004), (112), (200), (105), (211), (204), (116), and (220) lattice planes. The prominent peaks observed at 25.4° and 48.15° indicate that the synthesized TiO_2 nanoparticles are predominantly in the anatase phase [50, 51].

Based on the width of the XRD peak at <101>, the average crystallite size of the produced TiO_2 particles, was approximately 40.07 nm. Table 4 presents the unit cell volume and lattice characteristics of the synthesized TiO_2 nanoparticles. Notably, both the unit cell volume and the lattice characteristics of these nanoparticles align very closely with the experimental data for anatase TiO_2 [42].

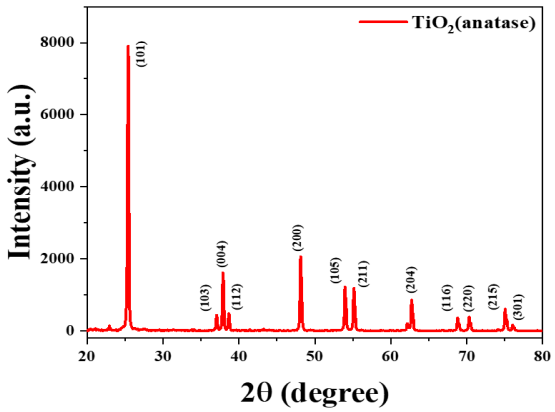

Fig. 7. XRD pattern of the synthesized TiO_2 nanoparticle

Table 3. XRD data of synthesized TiO_2 nanoparticle

Plane (hkl)	2θ (deg)	FWHM (rad)	Crystallite Size (nm)	Inter-planar Spacing (A°)
101	25.4	0.003508	40.07	3.50
103	37.04	0.003543	40.82	2.42
004	37.9	0.004076	35.56	2.37
112	38.67	0.005201	27.94	2.33
200	48.15	0.004016	37.40	1.89
105	53.99	0.004251	36.20	1.697
211	55.16	0.004363	35.45	1.66
204	62.78	0.005204	30.87	1.48
116	68.84	0.00548	30.83	1.36
220	70.36	0.005707	29.39	1.34

Table 4. Disparities between the produced TiO_2 nanoparticle's unit cell volume and lattice properties with experimental measurements

Sample	a (nm)	c (nm)	V (nm^3)
Synthesized TiO_2	0.377	0.9488	0.1349
Experimental [52]	0.3785	0.9514	0.1363
Deviation (%)	0.396%	0.273%	1.02%

3.2. SEM Analysis

The FESEM micrograph presented in Figure 8 illustrates the morphology and structural characteristics of the synthesized TiO_2 nanoparticles. The SEM images shown in Figures 8(a) and 8(b) reveal particles consistent in size and shape, although some agglomeration and elongated particles are evident alongside the predominantly spherical TiO_2 nanoparticles. Analysis using ImageJ software indicates that the average grain size of these nanoparticles is approximately 50.03 nm. The detailed distribution of the grain sizes of the produced TiO_2 nanoparticles is provided in Figure 9.

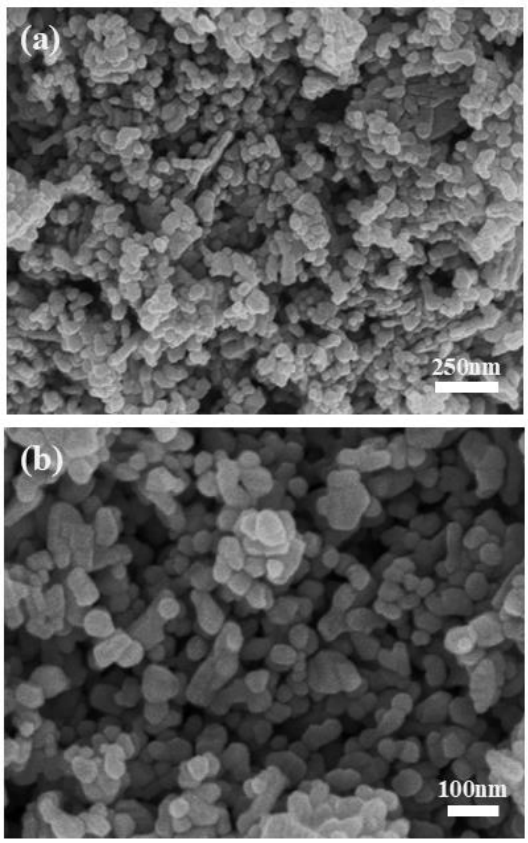

Fig. 8. The synthesized TiO_2 nanoparticles in a scanning electron microscope picture at (a) 50,000 magnification and (b) 100,000 magnification

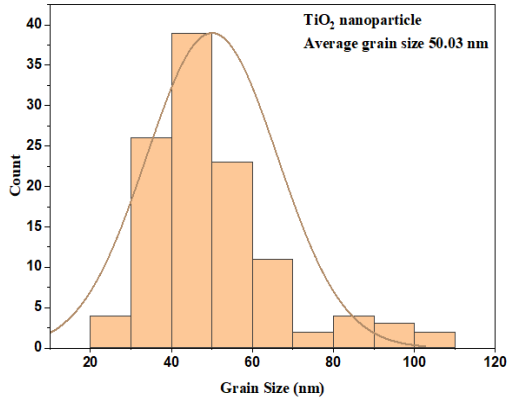

Fig. 9. Grain size distribution of the fabricated TiO_2 nanoparticles

3.3. Heat Transfer Analysis

The effects of nanofluid flow rate and nanoparticle concentration on heat transfer rate and the overall coefficient of heat transfer are demonstrated in Figures 10 and 11. Both the heat transfer rate and overall heat transfer coefficient rise in tandem with the volumetric concentration of nanoparticles and the flow rate of the nanofluid.

This enhancement is attributed to increased collisions between nanoparticles and a greater mass flow rate, which together improve thermal conductivity and other thermal properties. In addition to enhanced conductivity, dynamic phenomena such as Brownian motion, nanoparticle deposition, and micro-convection may also contribute to the observed improvements in heat transfer. These mechanisms facilitate local mixing and optimize the behavior of the thermal boundary layer [14].

The maximum values recorded during this experimental investigation are a heat transfer rate of 503.17 W and an overall heat transfer coefficient of 1141.64 $W/m^2 \cdot K$, achieved at a nanoparticle concentration of 0.3 vol.% and a flow rate of 12 l/min. In comparison to the base fluid, the average enhancements in heat transfer rate are 10.9%, 27.36%, and 38.25% for nanoparticle concentrations of 0.1 vol.%, 0.2 vol.%, and 0.3 vol.%, respectively. Similarly, the mean enhancements of overall heat transfer coefficient are 11.96%, 30.4%, and 42.25% at the same concentrations.

The effectiveness of the heat exchangers is significantly influenced by the volume concentration of nanoparticles, as illustrated in Figure 12. At nanoparticle concentrations of 0.1 vol.%, 0.2 vol.%, and 0.3 vol.%, the average increases in effectiveness compared to the base fluid (PGW) are 11.91%, 29.88%, and 41.82%, respectively. The highest effectiveness of the heat exchanger was observed at a nanofluid flow rate of 10 l/min. However, effectiveness declined with further increases in flow rate. Therefore, it can be concluded that maintaining the flow rate within permissible limits is crucial for optimizing heat exchanger performance.

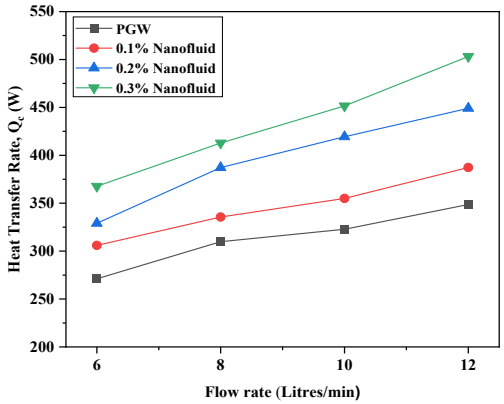

Fig. 10. Variation of the heat transfer rate with nanofluid (cold fluid) flow rate for base fluid and different nanoparticle volume concentrations at a constant hot fluid (tube side) flow

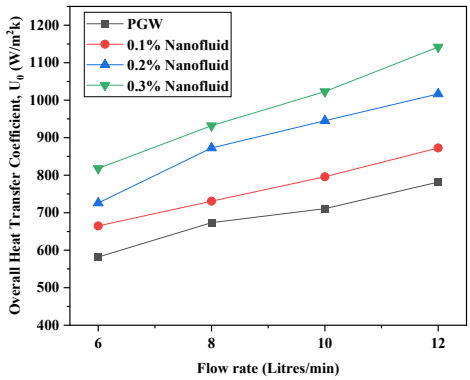

Fig. 11. Variation of the overall heat transfer coefficient with nanofluid (cold fluid) flow rate for base fluid and different nanoparticle volume concentrations at a constant hot fluid (tube side) flow

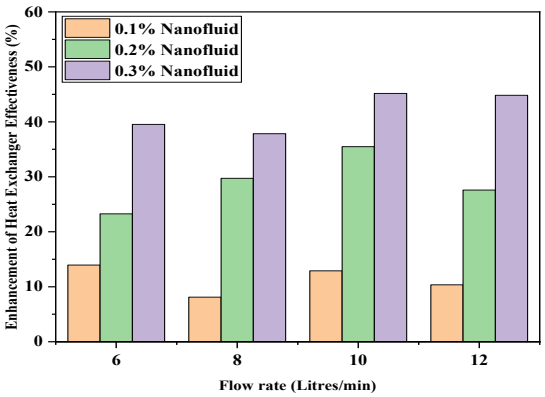

Fig. 12. Improvement in the heat exchanger effectiveness with nanofluid (cold fluid) flow rate for different nanoparticle volume concentrations at a constant hot fluid (tube side) flow

3.4. Exergetic Performance Analysis

Figures 13 and 14 illustrate how the volume concentration of nanoparticles affects exergy loss as well as dimensionless exergy loss. It is observed that due to the increment of the rate of flow of the nanofluid (the cold fluid), exergy loss as well as dimensionless energy loss increase. However, these losses significantly decrease with higher nanoparticle volume concentrations. This trend could be attributed to the increased irreversibility of the system at higher flow rates, resulting in greater exergy loss due to elevated frictional losses. Conversely, the incorporation of nanoparticles enhances the thermal properties of the fluid, promoting improved heat transfer and reducing exergy loss. Specifically, at concentrations of 0.1 vol.%, 0.2 vol.%, and 0.3 vol.%, the average exergy losses are 18.19%, 29.44%, and 45.39%, respectively.

Notably, for a nanofluid flow rate of 6 l/min with a nanoparticle concentration of 0.3 vol.%, the minimum dimensionless exergy loss was recorded at 0.0696, while maintaining a constant hot fluid flow rate of 12 l/min.

Figure 15 depicts the effects of nanoparticle volume concentration as well as nanofluid flow rate on exergetic effectiveness. It is noted that the exergetic effectiveness increases with higher nanoparticle concentrations but decreases with increased flow rates. At a nanofluid flow rate of 6 l/min, the maximum exergetic effectiveness of 30.34% is achieved at a 0.3 vol.% concentration of nanoparticles. The average increments in exergetic effectiveness at concentrations of 0.1 vol.%, 0.2 vol.%, and 0.3 vol.%, are 12.16%, 24.57%, and 33.75%, respectively.

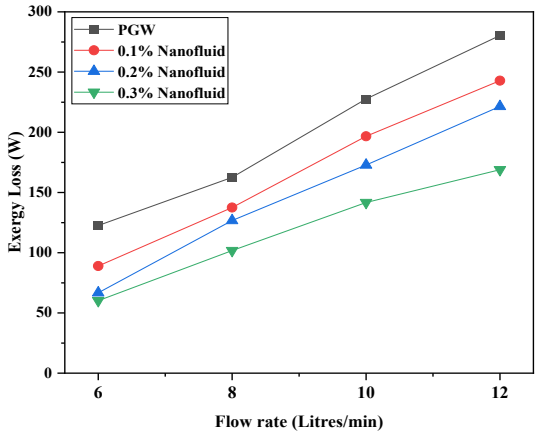

Fig. 13. Exergy loss versus nanofluid (cold fluid) flow rate for base fluid and different nanoparticle volume concentrations at a constant hot fluid (tube side) flow

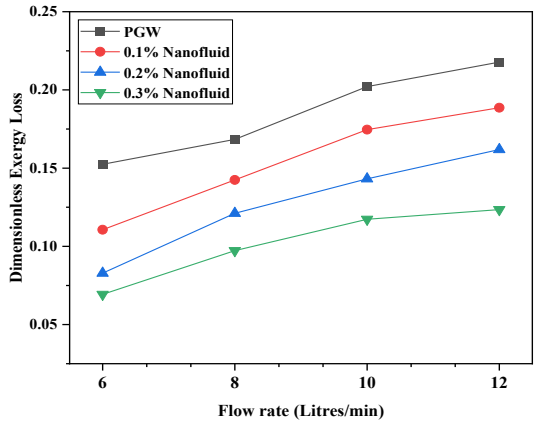

Fig. 14. Changes of dimensionless exergy loss with the flow rate of nanofluid (cold fluid) for the base fluid and various nanoparticle volume concentrations at a constant hot fluid (tube side) flow

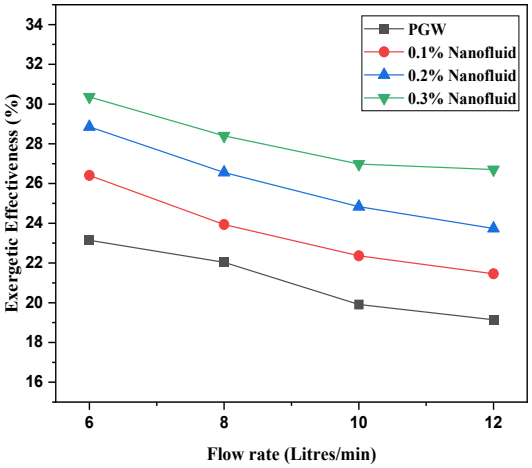

Fig. 15. Variation of exergetic effectiveness with the flow rate of nanofluid (cold fluid) for the base fluid and different nanoparticle volume concentrations at a constant hot fluid (tube side) flow

Exergetic effectiveness plays a crucial role in determining the exergetic sustainability index (SI), which increases with higher nanoparticle volume concentrations but decreases as the shell side (nanofluid) flow rate rises. The environmental impact factor (EIF) is inversely related to the sustainability index.

Figures 16 and 17 illustrate the effects of the volume concentration of nanoparticles and the flow rate of the nanofluid on both the SI and the EIF. With a 0.3 vol.% concentration and a flow rate of 6 l/min of nanofluid, the system achieves its maximum SI value of 0.44, accompanied by a minimum EIF value of 2.3. Moreover, a reduction in the EIF reveals that the system or process is more environmentally friendly.

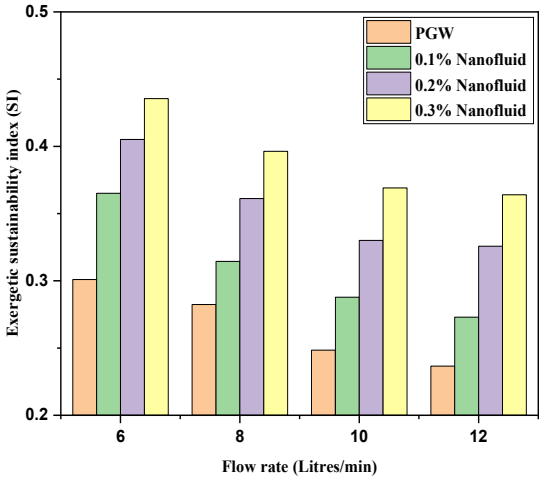

Fig. 16. Changes in the exergetic sustainability index (SI) for the base fluid and varying nanoparticle volume concentrations with respect to nanofluid flow rate at a constant hot fluid (tube side) flow

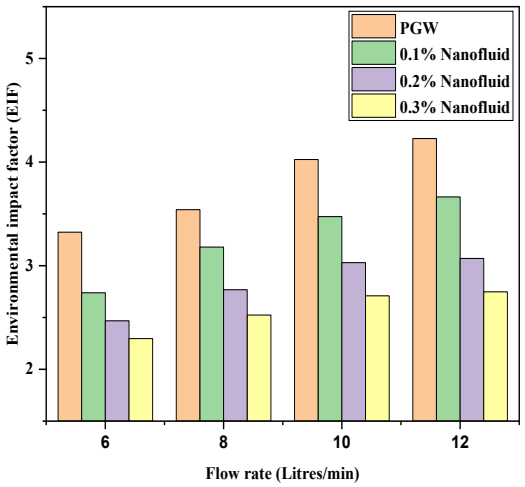

Fig. 17. Environmental impact factor (EIP) versus nanofluid flow rate for the base fluid and varying nanoparticle volume concentrations at a constant hot fluid (tube side) flow

4. Conclusions

This study presents a comprehensive exploration of heat transfer and exergetic performance using TiO_2-PGW nanofluids in a shell-and-tube heat exchanger. A key contribution of this work is the utilization of in-house synthesized TiO_2 nanoparticles, produced through a chemical process with H_2SO_4 and NH_4OH, aided by ultrasound. The XRD analysis confirmed the nanoparticles to be tetragonal anatase-phase TiO_2, revealing an average crystallite size of 40.07 nm and a grain size of 50.03 nm as observed via SEM. The following are the primary conclusions:

- As the flow rate of the nanofluid and nanoparticle volume concentration increased, both the overall heat transfer coefficient and the rate of heat transfer improved. At a nanoparticle concentration of 0.3 vol.% and a flow rate of 12 l/min, heat transfer rate increased by 44.39% and the overall heat transfer coefficient by 48.13% compared to the base fluid. The average increment in heat exchanger effectiveness at 0.1 vol.%, 0.2 vol.%, and 0.3 vol.% concentrations was 11.91%, 29.88%, and 41.82%, respectively.
- As the flow rate of the nanofluid increased, exergy loss and dimensionless exergy loss also increased. In contrast, both losses decreased significantly with higher nanoparticle volume concentrations.
- Exergetic effectiveness increased with the concentration of nanoparticles; however, it decreased as the flow rate of the nanofluid increased. At a flow rate of 6 l/min, the highest exergetic effectiveness of 30.34% was achieved with a 0.3 vol.% concentration of TiO_2 nanoparticles.

- The lowest environmental impact factor (2.3) and the highest energetic sustainability index (0.44) were observed at a nanoparticle concentration of 0.3 vol.% and a nanofluid flow rate of 6 l/min.

The findings of the experimental analysis indicate that while increasing both the volume concentration of nanoparticles and the flow rate of the nanofluid enhances overall heat transfer, it is essential to minimize the shell side flow rate of the nanofluid. This reduction is crucial for decreasing exergy loss and making the process more environmentally friendly and sustainable. This study enhances the understanding of PGW-based nanofluids, focusing on their environmental impact and energy efficiency, and suggests further research on hybrid nanofluids and their application in real-world energy systems.

5. Discussions

The results of this investigation unequivocally demonstrate the performance advantages offered by TiO_2-PGW nanofluids in a shell-and-tube heat exchanger configuration. The experimentally observed enhancement in heat transfer performance with increasing nanoparticle concentration is supported not only by improved thermal conductivity but also by several other mechanisms. In addition to enhancing convective heat transfer, the nanoparticles' Brownian motion and micro-convection effects promote thermal mixing at the microscale.

Although TiO_2 nanoparticles were effectively dispersed through prolonged stirring and sonication, the potential long-term impacts of sedimentation were not evaluated in this study and require further investigation. Due to equipment constraints, advanced surface characterization techniques, such as FTIR and zeta potential analysis, were not conducted to assess the surface chemistry and dispersion stability of the nanoparticles. Assuming temperature-independent behavior, thermophysical properties were calculated using established empirical models.

However, interfacial thermal resistance and temperature-dependent property variations were not taken into account, which may slightly influence accuracy. Furthermore, the long-term operational stability and reproducibility of the results were not assessed in this investigation. Future research will focus on the performance of TiO_2-PGW nanofluids under cyclic thermal loading and continuous operation.

Nomenclature

C_p	Specific heat [J/kg.K]
d	Tube diameter [m]
E	Exergy loss [W]
$\dot{m}$	Mass flow rate [Kg/s]
$\dot{Q}$	Heat transfer rate [J/s]
U	Overall heat transfer coefficient, [W/m^{2}k]
Ψ	Stream availability
η	Second law efficiency
ϕ	Volume concentration [%]
ΔT_m	Logarithmic mean temperature difference [K]
ρ	Density [kg/m^3]

Subscript

b_f	Base fluid
c	Cold fluid
h	Hot fluid
i	Inner side of the tube
n_p	Nanoparticles
o	Outer side of the tube

Acknowledgments

This research was carried out in the Department of Mechanical Engineering's Heat Transfer Lab, while TiO_2 nanoparticles were fabricated in the Department of Physics' postgraduate lab at Chittagong University of Engineering & Technology (CUET). The authors would like to express their gratitude to Dr. Md. Mohi Uddin (Professor, Department of Physics) for his kind assistance.

Funding Statement

This research did not receive any specific grant from funding agencies in the public, commercial, or not-for-profit sectors.

Conflicts of Interest

The author declares that there is no conflict of interest regarding the publication of this article.

Authors Contribution Statement

Gogan Dhar and Uschuas Dipta Das: Literature review, data analysis, preparation of the manuscript draft.

M. A. Mowazzem Hossain: Providing the idea for the article, editing the manuscript.

References

[1] Mukherjee, S., Poloju, V. and Mishra, P.C., 2023. Heat transfer, exergoeconomic performance and sustainability impact of a novel CuO+ MgO+ GO/Water ternary nanofluid. *Applied Thermal Engineering*, *235*, 121391. https://doi.org/10.1016/j.applthermaleng.2023.121391

[2] Wang, B., Klemeš, J.J., Li, N., Zeng, M., Varbanov, P. S. and Liang, Y., 2021. Heat exchanger network retrofit with heat exchanger and material type selection: A review and a novel method. *Renewable and Sustainable Energy Reviews*, *138*, 110479. https://doi.org/10.1016/j.rser.2020.110479

[3] Das, U.D., Hossain, M.A.M., Ahamed, J.U. and Razzaq, M.E.A., 2022. Heat transfer and exergy analysis of a shell and tube heat exchanger using PGW based ZnO nanofluids. *International Journal of Automotive and Mechanical Engineering*, 19(2), pp. 9773-9789. https://doi.org/10.15282/ijame.19.2.2022.12.0754

[4] Dhar, G., Raha, H.A., Razzaq, M.A. and Ahamed, J.U., 2019. Thermal Performance Improvement of a NFU Type Heat Exchanger Using Hybrid Nanofluids. *International Conference on Mechanical, Industrial and Materials Engineering 2019 (ICMIME2019)* 17-19 December, 2019, RUET, Rajshahi, Bangladesh.

[5] Etghani, M.M. and Baboli, S.A.H., 2017. Numerical investigation and optimization of heat transfer and exergy loss in shell and helical tube heat exchanger. *Applied Thermal Engineering*, 121, pp. 294–301. https://doi.org/10.1016/j.applthermaleng.2017.04.074

[6] Shahrul, I.M., Mahbubul, I.M., Saidur, R., Khaleduzzaman, S.S., Sabri, M.F.M. and Rahman, M.M., 2014. Effectiveness study of a shell and tube heat exchanger operated with nanofluids at different mass flow rates. *Numerical Heat Transfer; Part A: Applications*, 65(7), pp. 699–713. https://doi.org/10.1080/10407782.2013.846196

[7] Dhar, G., Razzaq, M.A., Ahamed, J.U. and Chakaraborty, P., 2020. Experimental Analysis for the Enhancement of Heat Transfer in a Tube Using Double Counter Twisted Tape. *5th International Conference on Mechanical Engineering and Renewable Energy 2019 (ICMERE2019)* 11–13 December, 2019, Chittagong, Bangladesh.

[8] Aghayari, R., Maddah, H., Zarei, M., Dehghani, M. and Kaskari Mahalle, S.G., 2014. Heat transfer of nanofluid in a double pipe heat exchanger. *International Scholarly Research Notices*, 2014(1), 736424. https://doi.org/10.1155/2014/736424

[9] Eneren, P., Aksoy, Y.T. and Vetrano, M.R., 2023. Practical challenges in nanofluid convective heat transfer inside silicon microchannels. *Energies*, 16(23), 7885. https://doi.org/10.3390/en16237885

[10] Wang, S., Wen, J. and Li, Y., 2008. An experimental investigation of heat transfer enhancement for a shell-and-tube heat exchanger. *Applied Thermal Engineering*, 29(11–12), pp. 2433–2438. https://doi.org/10.1016/j.applthermaleng.2008.12.008

[11] Devireddy, S., Mekala, C.S.R. and Veeredhi, V.R., 2016. Improving the cooling performance of automobile radiator with ethylene glycol water based TiO_2 nanofluids. *International Communications in Heat and Mass Transfer*, 78, pp. 121–126. https://doi.org/10.1016/j.icheatmasstransfer.2016.09.002

[12] Duong, N.T., Vuong, L.D., Son, N.M., Tuyen, H. van and Chuong, T. van, 2017. The synthesis of TiO_2 nanoparticles using sulfuric acid method with the aid of ultrasound. *Nanomaterials and Energy*, 6(2), pp. 82–88. https://doi.org/10.1680/jnaen.17.00009

[13] Sekrani, G. and Poncet, S., 2018. Ethylene- and propylene-glycol based nanofluids: A litterature review on their thermophysical properties and thermal performances. *Applied Sciences*, 8(11), 2311. https://doi.org/10.3390/app8112311

[14] Buschmann, M. H., Azizian, R., Kempe, T., Juliá, J. E., Martínez-Cuenca, R., Sundén, B. and Ala-Nissila, T., 2018. Correct interpretation of nanofluid convective heat transfer. *International Journal of Thermal Sciences*, *129*, pp. 504-531. https://doi.org/10.1016/j.ijthermalsci.2017.11.003

[15] Aksoy, Y.T., Enayati, F., Eneren, P. and Vetrano, M.R., 2025. Experimental study on enhanced heat transfer via nanoparticle depositions using TiO2-water nanofluid sprays. *Applied Thermal Engineering*, 264, 125450. https://doi.org/10.1016/j.applthermaleng.2025.125450

[16] Hamilton, R.L., 1962. Thermal conductivity of heterogeneous two-component systems. *Industrial and Engineering Chemistry Fundamentals*, 1(3), pp. 187–191. https://doi.org/10.1021/i160003a005

[17] Choi, S.U.S. 1995. Enhancing thermal conductivity of fluids with nanoparticles. In: Siginer DA, Wang HP, Eds., *Developments and Applications of Non-Newtonian Flows,* 66, pp. 99-105. https://www.osti.gov/servlets/purl/196525.

[18] Li, S., Eastman, J.A., Choi, U.S., Thompson, L.J. and Lee, S., 2011. Enhanced thermal conductivity through the development of nanofluids. *MRS Proceedings*, 457, pp. 3–11. https://doi.org/10.1557/PROC-457-3

[19] Masuda, H., Ebata, A., Teramae, K. and Hishinuma N., 1993. Alteration of thermal conductivity and viscosity of liquid by dispersing ultra-fine particles. dispersion of Al_2O_3, SiO_2, and TiO_2 ultra-fine particles. *Netsu Bussei*, 7(4), pp. 227–233.

[20] Cabaleiro, D., Nimo, J., Pastoriza-Gallego, M.J., Piñeiro, M.M., Legido, J.L. and Lugo, L., 2015. Thermal conductivity of dry anatase and rutile nano-powders and ethylene and propylene glycol-based TiO_2 nanofluids. *Journal of Chemical Thermodynamics,* 83, pp. 67–76. https://doi.org/10.1016/j.jct.2014.12.001

[21] Sundar, L.S., Ramana, E.V., Singh, M.K., Gracio, J. and A. Sousa, C.M., 2014. Preparation, thermal and rheological properties of propylene glycol and water mixture based Fe_3O_4 nanofluids. *Journal of Nanofluids*, 3(3), pp. 200–209. https://doi.org/10.1166/jon.2014.1108

[22] Hussein, A.M., Bakar, R.A., Kadirgama, K. and Sharma, K.V. 2014. Heat transfer augmentation of a car radiator using nanofluids. *Heat and Mass Transfer,* 50(11), pp. 1553–1561. https://doi.org/10.1007/s00231-014-1369-2

[23] Palanisamy, K. and Kumar, P.C.M., 2019. Experimental investigation on convective heat transfer and pressure drop of cone helically coiled tube heat exchanger using carbon nanotubes/water nanofluids. *Heliyon*, 5(5), e01705. https://doi.org/10.1016/j.heliyon.2019.e01705

[24] Jagadishwar, K. and Babu, S.S., 2017. Performance Investigation of Water and propylene glycol mixture based nano-fluids on automotive radiator for enhancement of heat transfer. *International Journal of Mechanical Engineering and Technology*, 8(7), pp. 822–833.

[25] Mohammadzadeh, A.M., Jafari, B. and Hosseinzadeh, K., 2025. Performance enhancement of disc-and-doughnut shell and tube heat exchangers through various tube layouts and ternary nanoparticle integration. *Applied Thermal Engineering*, 265, 125515. https://doi.org/10.1016/j.applthermaleng.2025.125515

[26] Mohammadzadeh, A.M., Jafari, B., Hosseinzadeh, K. and Paikar, E., 2025. Numerical investigation of segmental baffle design in shell and tube heat exchangers with varying inclination angles and spacing. *Scientific Reports*, *15*(1), 4683. https://doi.org/10.1038/s41598-025-87652-x

[27] Khedher, N.B., Hosseinzadeh, K., Abed, A.M., Khosravi, K., Mahdi, J.M., Sultan, H.S. and Talebizadehsardari, P., 2024. Accelerated charging of PCM in coil heat exchangers via central return tube and inlet positioning: A 3D analysis. *International Communications in Heat and Mass Transfer*, 152, 107275. https://doi.org/10.1016/j.icheatmasstransfer.2024.107275

[28] Paikar, M., Hosseinzadeh, K., Kermani, J.R. and Ganji, D.D., 2024. Hydrothermal assessment of a double-pass shell and tube heat exchanger in the presence of blade turbulators with different configurations. *International Journal of Thermofluids*, 21, 100577. https://doi.org/10.1016/j.ijft.2024.100577

[29] Moghaddam, M.E., Abandani, M.H.S., Hosseinzadeh, K., Shafii, M.B. and Ganji, D.D., 2022. Metal foam and fin implementation into a triple concentric tube heat exchanger over melting evolution. *Theoretical and Applied Mechanics Letters*, 12(2), 100332. https://doi.org/10.1016/j.taml.2022.100332

[30] Mohammadzadeh, A.M., Jafari, B. and Hosseinzadeh, K., 2024. Comprehensive numerical investigation of the effect of

various baffle design and baffle spacing on a shell and tube heat exchanger. *Applied Thermal Engineering*, 249, 123305. https://doi.org/10.1016/j.applthermaleng.2024.123305

[31] Ahamed, J.U., Saidur, R., Masjuki, H.H., Mekhilef, S., Ali, M.B. and Furqon, M.H., 2011. An application of energy and exergy analysis in agricultural sector of Malaysia. *Energy Policy*, 39, pp. 7922–7929. https://doi.org/10.1016/j.enpol.2011.09.045

[32] Hossain, S., Chowdhury, H., Chowdhury, T., Ahamed, J.U., Saidur, R., Sait, S.M. and Rosen, M.A., 2020. Energy, exergy and sustainability analyses of Bangladesh's power generation sector. *Energy Reports*, 6, pp. 868-878. https://doi.org/10.1016/j.egyr.2020.04.010

[33] Gupta, S.K., Verma, H. and Yadav, N., 2022. A review on recent development of nanofluid utilization in shell & tube heat exchanger for saving of energy. *Materials Today: Proceedings*, 54, pp. 579-589. https://doi.org/10.1016/j.matpr.2021.09.455

[34] Razzaq, M.A., Ahamed J.U. and Hossain, M.A.M., 2020. Effect of TiO_2/MO nano-lubricant on energy and exergy savings of an air conditioner using blends of R22/R600a. *International Journal of Automotive and Mechanical Engineering*, 17(4), pp. 8283–8297. https://doi.org/10.15282/ijame.17.4.2020.06.0626

[35] Prajapati, P., Raja, B.D., Savaliya, H., Patel, V. and Jouhara, H., 2024. Thermodynamic evaluation of shell and tube heat exchanger through advanced exergy analysis. *Energy*, 292, 130421. https://doi.org/10.1016/j.energy.2024.130421

[36] Romero, J.C. and Linares, P., 2014. Exergy as a global energy sustainability indicator. A review of the state of the art. *Renewable and Sustainable Energy Reviews*, 33, 427–442. https://doi.org/10.1016/j.rser.2014.02.012

[37] Durmuş, A., 2004. Heat transfer and exergy loss in cut out conical turbulators. *Energy Conversion and Management*, 45(5), pp. 785–796. https://doi.org/10.1016/S0196-8904(03)00186-9

[38] Dizaji, H.S., Khalilarya, S., Jafarmadar, S., Hashemian, M. and Khezri, M., 2016. A comprehensive second law analysis for tube-in-tube helically coiled heat exchangers. *Experimental Thermal and Fluid Science*, 76, pp. 118–125. https://doi.org/10.1016/j.expthermflusci.2016.03.012

[39] Khairul, M.A., Alim, M.A., Mahbubul, I.M., Saidur, R., Hepbasli, A. and Hossain, A., 2014. Heat transfer performance and exergy analyses of a corrugated plate heat exchanger using metal oxide nanofluids. *International Communications in Heat and Mass Transfer*, 50, 8–14. https://doi.org/10.1016/j.icheatmasstransfer.2013.11.006

[40] Esfahani, M.R. and Languri, E.M., 2017. Exergy analysis of a shell-and-tube heat exchanger using graphene oxide nanofluids. *Experimental Thermal and Fluid Science*, 83, pp. 100-106. https://doi.org/10.1016/j.expthermflusci.2016.12.004

[41] Pak, B.C. and Cho, Y.I., 1998. Hydrodynamic and heat transfer study of dispersed fluids with submicron metallic oxide particles. *Experimental Heat Transfer*, 11(2), pp. 151–170. https://doi.org/10.1080/08916159808946559

[42] Smyth, J.R. and Bish, D.L., 1988. *Crystal structures and cation sites of the rock-forming mineral.* First Edition. Boston, Allen and Unwin.

[43] Torres, P. and Rurali, R., 2019. Thermal conductivity of rutile and anatase TiO_2 from First-Principles. *Journal of Physical Chemistry C*, 123(51), pp. 30851–30855. https://doi.org/10.1021/acs.jpcc.9b09299

[44] Smith, S.J., Stevens, R., Liu, S., Li G., Navrotsky, A., Boerio-Goates, J. and Woodfield, B.F., 2009. Heat capacities and thermodynamic functions of TiO_2 anatase and rutile: Analysis of phase stability. *American Mineralogist*, 94(2–3), pp. 236–243. https://doi.org/10.2138/am.2009.3050

[45] Hussein, A.M., Bakar, R.A., Kadirgama, K. and Sharma, K.V., 2013. Experimental measurement of nanofluids thermal properties. *International Journal of Automotive and Mechanical Engineering,* 7(June), pp. 850–863. http://dx.doi.org/10.15282/ijame.7.2012.5.0070

[46] Propylene Glycol based Heat-Transfer Fluids, The Engineering ToolBox, Mar.30, 2020. [Online]. Available:

https://www.engineeringtoolbox.com/propylene-glycol-d_363.html.

[47] Holman, J.P., 2010. *Heat Transfer*: Tenth Edition, New York, The McGraw-Hill companies, Inc.

[48] Arslan, E. and Aktas, M., 2020. 4E analysis of infrared-convective dryer powered solar photovoltaic thermal collector. *Solar Energy*, 208, pp. 46–57. https://doi.org/10.1016/j.solener.2020.07.071

[49] Gojak, M. and Bajc, T., 2019. Thermodynamic sustainability assessment for heating of residential building. *E3S Web of Conferences 111 CLIMA 2019*, 04028.

[50] Pratheepa, M.I. and Lawrence, M., 2017. X-Ray diffraction analyses of titanium dioxide nanoparticles. *International Journal of Scientific Research in Science and Technology*, 3(11), pp. 83-88.

[51] Theivasanthi, T. and Alagar, M., 2013. Titanium dioxide (TiO_2) nanoparticles XRD analyses: An insight. arXiv preprint arXiv:1307.1091. https://doi.org/10.48550/arXiv.1307.1091

[52] Hanaor, D., Sorrell, C., Hanaor, D.A.H. and Sorrell, C.C., 2011. Review of the anatase to rutile phase transformation. *Journal of Materials Science*, 46(4), pp. 855-874. https://doi.org/10.1007/s10853-010-5113-0